Catalysis Today xxx (xxxx) xxx

Contents lists available at ScienceDirect

Catalysis Today

journal homepage: www.elsevier.com/locate/cattod

Influence of Cu-speciation in mordenite on direct methane to methanol conversion: Multi-Technique characterization and comparison with NH_3 selective catalytic reduction of NO_x

Dimitrios K. Pappas [a,*], Karoline Kvande [a], Maria Kalyva [a], Michael Dyballa [a], Kirill A. Lomachenko [b], Bjørnar Arstad [c], Elisa Borfecchia [d,*], Silvia Bordiga [d], Unni Olsbye [a], Pablo Beato [e,*], Stian Svelle [a]

[a] Center for Materials Science and Nanotechnology (SMN), Department of Chemistry, University of Oslo, 1033 Blindern, 0315 Oslo, Norway
[b] European Synchrotron Radiation Facility, 71 avenue des Martyrs, CS 40220, 38043 Grenoble Cedex 9, France
[c] SINTEF Industry, Department of Process Technology, Forskningsveien 1, 0373 Oslo, Norway
[d] Department of Chemistry, NIS Center and INSTM Reference Center, University of Turin, via P. Giuria 7, 10125 Turin, Italy
[e] Haldor Topsøe A/S, Haldor Topsøes Allé 1, DK-2800 Kgs. Lyngby, Denmark

ARTICLE INFO

Keywords:
Zeolite
Methane activation
XPS
SCR
Characterization

ABSTRACT

The direct conversion of methane to methanol has the potential of substantially reducing methane emissions and flaring, as such a process might provide an alternative for remote natural gas locations. In this report, we investigate the performance of a range of Cu-exchanged mordenite zeolites as active materials for such a reaction, employing a stepwise protocol comprising activation in oxygen, methane loading, and methanol extraction with steam. We employ *in situ* HERFD XANES, FT-IR spectroscopy with CO as probe molecule, and XPS to investigate the Cu species in the zeolites during the process. The activity of the materials is investigated both for methane to methanol conversion and NH_3 Selective Catalytic Reduction of NO_x. It is demonstrated that, despite the fact that the same zeolite materials are active both for NH_3-SCR and direct methane to methanol conversion, the active site requirements for these two reactions are different.

1. Introduction

The direct conversion of methane to methanol has been the topic of substantial research efforts over the past years, due to the potential for economic and enviromental impact it holds. Such a process can substantially reduce methane emissions and flaring since it might provide a feasible alternative for utilization of remote natural gas. Different approaches have been investigated for the conversion, with emphasis on heterogenous catalysts, which are the most suitable for such processing. One of the most promising options, running at mild conditions and exhibiting very high selectivity, is the direct stepwise conversion of methane to methanol over Cu-exchanged zeolites, inspired by methanotrophic enzymes found in nature [1–4]. Upon O_2 activation, Cu ions exchanged into the confined environment of the zeolite framework form Cu_xO_y species, able to cleave the C–H bond of methane. In this way, upon reaction with methane, a surface bound reaction intermediate is stabilized and protected from further reaction, either on the Cu-oxo centre or the Brønsted acid sites present in the zeolite [5–8]. To date, different zeolite frameworks, such as MFI, MOR, CHA, MAZ, FAU and FER have been investigated for the conversion. Cu-MOR zeolites are among the most active materials, as shown in literature [2,9–16]. The direct conversion of methane to methanol (DMTM) involves three consecutive steps: high temperature activation in O_2, CH_4 loading at 200 °C, and finally extraction of the products with steam.

The mordenite (MOR) topology comprises straight 12MR channels with a cross section of 7.0 × 6.5 Å and perpendicular 8MR side pockets with a cross section of 5.7 × 2.6 Å. The speciation of Cu in the MOR framework has been investigated extensively since the early 1990s with Kuroda et al. reporting divalent Cu ions with tetragonal symmetry, which form dimeric species [17]. Vanelderen et al. identified Cu^{II} species in O_2-activated Cu-MOR as isolated ions and bent binuclear oxo-complexes $[Cu(\mu\text{-}O)Cu]^{2+}$ [18]. The location of the latter species is proposed to be in the 8MR, inside the 8MR channel, and/or 8MR window adjacent to the 12MR main channel; each location corresponding to

* Corresponding authors.
E-mail addresses: dimitrios.pappas@smn.uio.no (D.K. Pappas), elisa.borfecchia@unito.it (E. Borfecchia), pabb@topsoe.com (P. Beato).

https://doi.org/10.1016/j.cattod.2020.06.050
Received 15 October 2019; Received in revised form 20 May 2020; Accepted 13 June 2020
Available online 23 June 2020

a different reactivity [19,20]. The existence of bridging oxygen was supported by Alayon et al. by comparing high temperature activation in inert He and oxidative O_2. Using XAS, it was shown that in the case of O_2 activation, two Cu neighbors with 2.29 Å distance are bridged by one oxygen. In contrast, this is not the case after He activation [21]. More support in favor of a mono(μ-oxo)dicopper core rather than a bis(μ-oxo) dicopper species can be found in the literature [21–23]. In a previous study from our group, we investigated the nature of Cu ions in H-MOR samples with Si/Al ratios of 11 and 7 and with different Cu loadings with a variety of methods. X-ray absorption spectroscopy (XAS), high energy resolution fluorescence detected X-ray absorption near edge spectroscopy (HERFD XANES) coupled with multivariate curve resolution (MCR) as well as DMTM activity measurements were employed [15]. Both active and inactive framework-coordiated-Cu^{II} (fw-Cu^{II}) species were found to coexist after O_2 activation, while a very specific fw-Cu^{II} moiety was identified as the active site for methane activation. This active species is characterized by a high resistance toward self-reduction during activation in inert gas flow, and its formation is highly favored in a paricular Cu-MOR sample with Si/Al = 7 and Cu/Al = 0.18 (denoted 0.18Cu-HMOR(7)) [15]. These results were confirmed by Brezicki et al., reporting a first shell coordination number of 2.9 ± 0.2 for Cu, consistent with $[Cu(\mu\text{-}O)Cu]^{2+}$ or $[Cu(\textit{trans}\text{-}\mu\text{-}1,2\text{-}O_2)Cu]^{2+}$ [16]. Grundner et al. have suggested trinuclear Cu-oxo clusters $[Cu_3(\mu\text{-}O)_3]^{2+}$ located in the side pocket of MOR as the active site for DMTM conversion [12]. Beyond mono-, di- and trinuclear Cu active sites, theoretical studies have considered even larger clusters, with four and even five Cu atoms. It has been suggested that higher nuclearity and more extensive Cu-O bonding increase the cluster stability [24].

In this contribution, we extend the characterization of our previously investigated set of Cu-HMOR samples with different Si/Al and Cu/Al ratios [15,25,26]. Herein we show the effect of activation in He as monitored by *in situ* HERFD XANES and how this helps us to identify the different environments for Cu ions in the samples. In addition, by utilizing FT-IR spectroscopy with CO as probe molecule, we observe the effect of the compositional characterisitics on the formation of mono and dicarbonyl adducts, thus complementing the HERFD XANES results. Moreover, we study two samples from each Si/Al ratio, both in the as synthesized state as well after activation in air at 500 °C using X-ray photoelectron spectroscopy (XPS). Finally, we compare the NO_x conversion rates of these Cu-HMOR samples in the NH_3-assisted selective catalytic reduction (SCR) of NO_x. We note, however, that a detailed investigation of these materials in the context of NH_3-SCR is beyond the scope of the present work. With this comparison, we merely search for analogies and differences in the performance of the investigated samples for another widely investigated redox chemistry. We seek to highlight how the active site requirements are very different for DMTM and the NH_3-SCR activity, even though both reactions are catalyzed by the same materials.

The overall goal of the study is to demonstrate how the speciation and thus performance of Cu-HMOR in DMTM depends strongly on both the composition of the materials (Si/Al and Cu/Al ratios) and preparation methods. Further, we wish to shed light on why one particular Cu-HMOR sample (Cu/Al = 0.18; Si/Al = 7) displays higher DMTM performance per Cu than other, seemingly similar materials.

2. Materials and methods

2.1. Preparation of Cu-exchanged MOR zeolites

The preparation of the Cu-exchanged MOR samples used herein was descibed in detail in previous publications [15,25]. In short, commercial zeolites from from Zeolyst Inc. designated CBV21A (NH_4-MOR, Si/Al = 11) and CBV10ADS (Na-MOR, Si/Al = 7) were used. Prior to Cu loading, however, these zeolites were exchanged into their proton form with NH_4NO_3, followed by calcination to remove the NH_3 (500 °C in air for 8 h). Liquid ion exchange with Cu was performed using a Cu^{II} acetate solution at a pH between 5.2–5.7 while stirring at RT for 16 h. Finally, the solution was removed by centrifugation and the material was washed with deionized H_2O at least three times before drying at ca. 80 °C. The samples designations as well as their composition and BET surface area are listed in Table 1. Additional characterization of the studied samples, such as MAS NMR, SEM, EDX and XRD can be found in previous works [15,25,26].

2.2. Direct methane to methanol (DMTM) activity measurements

The activity of Cu-MOR zeolites in the DMTM conversion was evaluated in a quartz plug flow reactor (I.D. = 6 mm) placed in a tubular oven [15,25]. The temperature was monitored by a quartz sheathed thermocouple placed in the centre of the bed. For each measurement, 100 mg of zeolite was utilized. The sample was pressed in pellets, ground and sieved in order to obtain uniform particles in the 250–425 μm range. The stepwise DMTM process included the following three steps: (i) activation in neat O_2 flow (15 mL/min) at 500 °C; (ii) reaction with neat CH_4 (15 mL/min) at 200 °C; (iii) extraction of methanol with 10 % H_2O in a flow of 10 % Ne/He (total flow 15 mL/min) at 200 °C. Between each step, the materials were flushed with He (15 mL/min) and the temperature ramps up/down were performed with a constant ramp of 5 °C/min. During CH_3OH extraction, the effluent was analysed by a Hewlett Packard 6890/5972 GC–MS system.

2.3. High energy resolution fluorescence detected X-ray absorption near edge spectroscopy (HERFD XANES) measurements

HERFD XANES measurements were performed at the ID26 beamline at the ESRF. The spectra were collected in fluorescence mode, detecting only photons with energy corresponding to the maximum intensity of the Cu $K_{\beta 1,3}$ emission line (~ 8906 eV). This energy selection was performed using five Si [553] analyser crystals (θ = 79.92°), set up in vertical Rowland geometry, resulting in a spectral resolution of 1.06 eV (elastic peak). The crystals were spherically bent following the Johann scheme to focus the fluorescence radiation onto an APD detector. For the incident beam, a flat double-crystal Si [311] monochromator was employed. For each spectrum, the acquisition time was set to 2 min.

The measurements were conducted using a well-established gas-flow setup, based on the Microtomo reactor cell (developed by the ESRF Sample Environment team) [27], that allows precise control of the gas composition and the temperature inside the cell, as described in detail in our previous work [28–31]. The Cu-MOR samples were prepared in the form of self-supporting wafers (ca. 100 mg of sample) and fixed inside the reactor cell. *in situ* experiments during He activation were performed by heating the samples from 60 °C to 500 °C with a heating ramp of 5 °C/min in a He flow of 100 mL/min. After stabilization for 30 min at 500 °C in He, five scans were collected and averaged to obtain a higher-quality HERFD XANES spectrum. All the collected HERFD XANES spectra were normalized to unity edge jump using the Athena software from the Demeter package [32].

2.4. Fourier Transformed Infrared (FTIR) spectroscopy with CO as probe molecule

A Bruker Vertex 80 instrument with a Mercury-Cadmium-Telluride

Table 1
Cu-HMOR sample names, Cu/Al, Si/Al, Cu loading in μmol/g and BET surface area in m^2/g.

Sample	Cu/Al	Si/Al	Cu (μmol/g)	BET (m^2/g)
0.18Cu-HMOR(7)	0.18	7	367	440
0.24Cu-HMOR(7)	0.24	7	504	440
0.28Cu-HMOR(11)	0.28	11	389	470
0.36Cu-HMOR(11)	0.36	11	500	460

(MCT) detector was used for the FTIR spectroscopy measurements. A quartz cell with KBr windows was employed. The as prepared Cu-exchanged MOR samples were prepared as self-supported thin wafers with a weight of 15 mg, and this wafer was fixed in a gold envelope. Prior to the measurements, the samples were pretreated under vacuum at 150 °C for 1 h, 300 °C for 1 h and 450 °C for 1 h. The CO adsorption measurements were conducted at room temperature by using incremental doses of CO from 20 μbar up to a total pressure of 20 mbar.

2.5. X-ray photoelectron spectroscopy (XPS) measurements

XPS spectra were collected both for as prepared and activated materials. Activation was carried out in 10 % O_2/Ar flow at 500 °C, for 3 h in an adjacent pre-treatment cell attached to the XPS instrument, from which the samples were transferred to the analysis chamber without breaking vacuum. XPS analysis of the samples was performed on a Kratos Axis Ultra^{DLD} instrument using monochromatic Al Kα radiation ($h\nu$ = 1,486.6 eV) at 15 kV and 10 mA. The pass energies for the high-resolution scan was 20 eV. The pressure in the chamber was maintained below 8×10^{-9} mbar during the analysis. The binding energy values were corrected with reference to the carbon C 1s = 284.6 eV.

2.6. NH_3-selective catalytic reduction (SCR) activity measurements

The NH_3-SCR reaction was performed using a U-shaped quartz reactor (ID = 6 mm). Prior to the reaction, the sample was pressed, ground in a mortar and sieved, obtaining a uniform particle distribution in the 250–420 μm range. 100 mg was packed in the reactor and a quartz sleeve containing the thermocouple was inserted in the middle of the bed. Before catalytic tests, the samples were activated in 10 % O_2/He (50 mL/min) for 1 h at 550 °C. Then the temperature was lowered to 150 °C and the material was flushed with He for ca. 60 min (50 mL/min). The SCR reaction mixture was composed of 924 ppm NH_3, 903 ppm NO, and 8.6 % O_2 balanced in He and N_2. The total flow was 115 mL/min and the gas hourly space velocity (GHSV) about 19,000 h^{-1}. Measurements of the feed gas composition was done by bypassing the reactor before activity tests. The ion currents corresponding to NO, NO_2, N_2O, H_2O and NH_3 were monitored using a mass spectrometer at the reactor outlet and the NO conversion was calculated. The NH_3-SCR was performed in the temperature range from 150 to 500 °C with 50 °C increments; at each temperature the NO conversion was calculated after achieving steady state after ca. 30–45 min.

3. Results and discussion

3.1. Performance of Cu-HMOR zeolites for the DMTM conversion

The DMTM activity of the investigated samples is shown in Fig. 1; there the CH_3OH yield in μmol/g (Fig. 1a) and molCH_3OH/molCu (Fig. 1b) are displayed. It is evident that among the investigated samples, the Cu-HMOR with Cu/Al = 0.18 and Si/Al = 7 (0.18Cu-HMOR(7) produces the highest amount of CH_3OH per gram and per mol of Cu, i.e. 170 μmol/g and 0.47 molCH_3OH/molCu. The remaining samples exhibit an increasing CH_3OH yield (μmol/g) (Fig. 1a) with increasing Cu loading (Table 1), with the following order 0.28Cu-HMOR(11) < 0.36Cu-HMOR(11) < 0.24Cu-HMOR(7). However, when normalizing to the Cu loading (Fig. 1b) the samples exhibit very similar productivities in units of molCH_3OH/molCu, around 0.26, with an exception for 0.18Cu-HMOR (7), as noted above. In our previous work, combining *operando* XAS and HERFD XANES coupled with MCR analysis and activity measurements, we have elucidated, to an extent, this difference in performance [15]. This was attributed to a higher population of dicopper sites for the 0.18Cu-HMOR(7), compared to the rest of the samples under identical activation conditions. These species have been identified as $[Cu(\mu\text{-}O)Cu]^{2+}$ or $[Cu(trans\text{-}\mu\text{-}1,2\text{-}O_2)Cu]^{2+}$, based also on other reports [16]. These sites possess a higher resistance to self-reduction compared to other Cu species present [15].

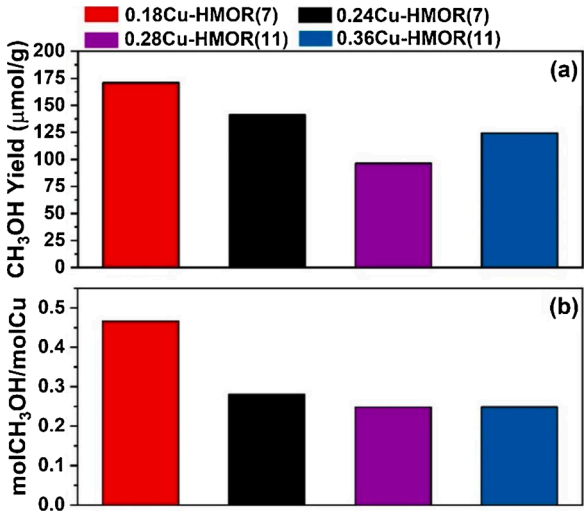

Fig. 1. a) CH_3OH yield in μmol/g and **b)** normalized productivity in mol-CH_3OH/molCu for the 0.18Cu-HMOR(7), 0.24Cu-HMOR(7), 0.28Cu-HMOR(11) and 0.36Cu-HMOR(11) samples. The materials were tested under identical reaction conditions: O_2 activation at 500 °C for 480 min, CH_4 loading at 200 °C for 360 min and H_2O-assisted extraction at 200 °C with 10 % H_2O.

3.2. HERFD XANES of He-activated Cu-HMOR zeolites

In situ HERFD XANES was employed to assess the oxidation state, average coordination, and ultimately the extent of self-reduction for selected Cu-HMOR samples during activation in He at 500 °C. Although He-activation does not yield DMTM activity (see SI ref. [15]), it facilitates the discrimination of the different Cu species present in the samples based on their different resistance to self-reduction, resulting in different Cu^I abundances at the same conditions. Indeed, much better contrast is observed in the XANES between Cu^{II} and Cu^I species rather than between Cu^{II} moieties with slightly different local structures, which are present after the O_2-activation step included in the standard DMTM

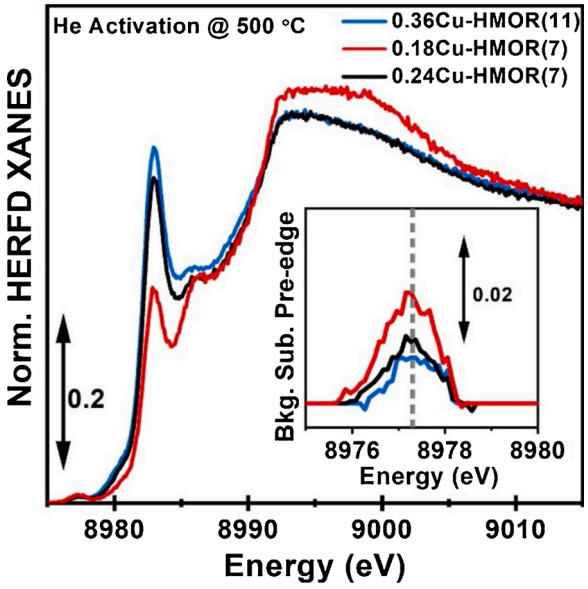

Fig. 2. Cu K-edge HERFD XANES of 0.18Cu-HMOR(7), 0.24Cu-HMOR(7) and 0.36Cu-HMOR(11) after He activation at 500 °C. The inset reports the background-subtracted normalized intensity of the 1s→3d pre-edge peak, which is characteristic of Cu^{II} ions.

protocol [15,25].

The spectra, after stabilization of the XAS features, are shown in Fig. 2. He activation is reported in the literature to result in a Cu^{I}-containing state, evidenced by the pronounced peak at 8983 eV corresponding to the 1s → 4p transitions of Cu^{I} ions (at lower energy compared to Cu^{II}). Cu^{I}-containing species are formed as a result of the self-reduction [21,28,31,33–36]. However, Cu^{II}-containing species, withstanding self-reduction, are also present after He activation at 500 °C. These are evidenced by the peak at 8986 eV, assigned to 1s → 4p transitions of Cu^{II} ions, as well as by the pre-edge peak at 8977 eV stemming from dipole-forbidden 1s → 3d transitions of Cu^{II} ions (Fig. 2 inset). From the spectra of the He-activated 0.18Cu-HMOR(7), 0.24Cu-HMOR(7) and 0.36Cu-HMOR(11) illustrated in Fig. 2, it is immediately evident that different degrees of self-reduction have occurred during the He activation protocol. The shape and intensity of the peak at 8983 eV, assigned to Cu^{I}-containing species, is diagnostic for quasi linear Cu^{I} species [37].

From Fig. 2 the more active 0.18Cu-HMOR(7) appears to be more resistant to reduction compared to the other two samples. In fact, for all the samples, the amount of Cu^{I} present after He activation is inversely proportional to their productivities in units of molCH_3OH/molCu: (0.18Cu-HMOR(7) > 0.24Cu-HMOR(7) > 0.36Cu-HMOR(11)). In addition, the higher intensity of the post-edge resonance at ca. 8995 eV, referred to as the white line (WL) peak, seen for the outperforming sample, indicates a higher average coordination number for Cu species, possibly due to the contribution of a significant population of dimeric Cu^{II}-oxo species that can withstand self-reduction. These results (obtained for Cu-HMOR samples) contradict the correlation between activity and reducibility exhibited for Cu-SSZ-13 and Cu-FER shown in our previous works [29,30]. However, we have also previously quantitatively identified the nature of the active site in Cu-HMOR as a self-reduction resistant fw-Cu^{II} with a nuclearity of two [15]. These species resist self-reduction up to 400 °C in He flow, which is consistent with the higher stability of multimeric species, compared to monomeric ones which exist in Cu-SSZ-13 [38]. The existence of these species as the active component for DMTM in Cu-HMOR rationalizes the obtained spectra in Fig. 2. On the other hand, in the case of Cu-SSZ-13, monomeric $[CuOH]^{+}$ species have been identified as the precursors to a pool of active sites [30]. The reducibility of such species is higher, compared to the $[Cu(\mu\text{-}O)Cu]^{2+}$ or/and $[Cu(trans\text{-}\mu\text{-}1,2\text{-}O_2)Cu]^{2+}$ proposed to exist in Cu-MOR. This can be attributed to various reasons, such as the local coordination of Cu in the different topologies, second-sphere effects, as well as different Cu distribution and mobility. However, a definitive explanation would require further in-depth studies across a large library of samples covering large ranges of both composition and topology.

3.3. CO-IR measurements of Cu-exchanged MOR samples

FTIR spectroscopy of adsorbed CO has been utilized to further assess abundance and nature of reducible Cu species in the Cu-HMOR samples studied herein. Importantly, at room temperature, CO preferentially probes Cu^{I} and does not interact visibly with Cu^{II} species [29,39–42]. Prior to the measurements, the samples were activated in vacuum at

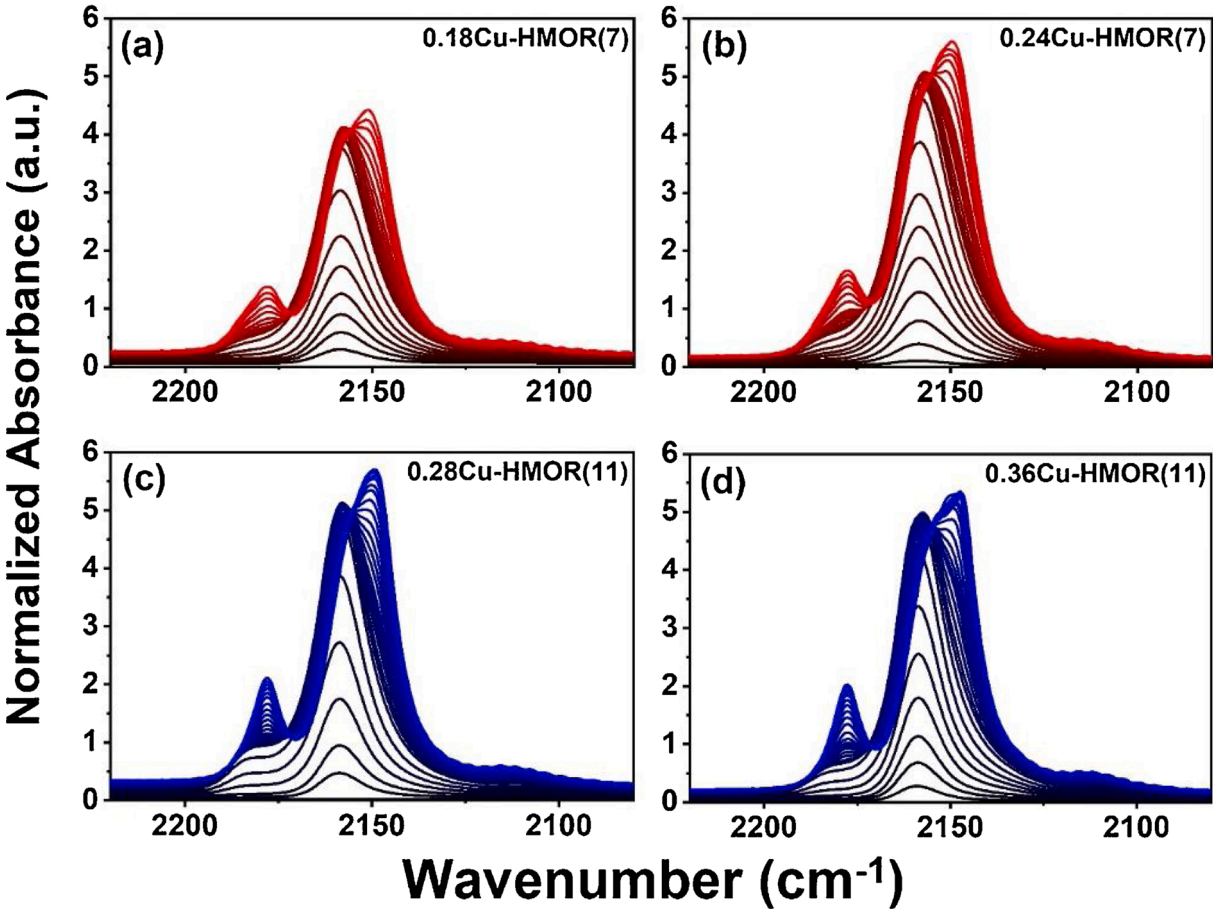

Fig. 3. FTIR spectra of CO dosed at RT on **a)** 0.18Cu-HMOR(7) **b)** 0.24Cu-HMOR(11) **c)** 0.28Cu-HMOR(11) and **d)** 0.36Cu-HMOR(11). The spectra are collected during incremental doses of CO from 20 μbar up to a total pressure of 20 mbar. Prior to the measurements, the samples were activated in vacuum at 150 °C for 1 h, 300 °C for 1 h and 450 °C for 1 h. The reported spectra are background-subtracted and first normalized to the zeolite framework vibrational modes and then to the Cu wt. %.

150, 300, and 450 °C for one hour at each temperature, a protocol leading to self-reduction. The spectra obtained at incremental CO pressures from 20 μbar to 20 mbar, carried out at room temperature (RT) for the four samples, are reported in Fig. 3a-d. Again, at RT, CO is only adsorbed on Cu^{I} sites, while its interaction with Brønsted acid sites and Cu^{II} species is suppressed, thus resulting in more easily interpretable IR spectra. In Fig. 3 at low CO pressures, the peak at 2157 cm^{-1} is evident for all the samples and is assigned to monocarbonyl species interacting with Cu^{I} ($Cu^{I}\cdots CO$) [39]. When increasing the CO pressure, two additional peaks at 2178 and 2151 cm^{-1} develop. These are assigned to the symmetric and asymmetric CO stretching modes of dicarbonyl species ($Cu^{I}\cdots(CO)_2$), respectively [29,39,42]. Interestingly, even though the spectra have been normalized to the Cu loading, differences in the intensity of the peaks can be observed among the samples. Initially, focusing on the peak at 2157 cm^{-1} assigned to $Cu^{I}\cdots CO$ we observe that the samples with Si/Al ratio of 11 (0.28Cu-HMOR(11) and 0.36Cu-MOR (11)) as well as the 0.24Cu-HMOR(7) exhibit very similar intensities of the peak. In contrast, the highly active 0.18Cu-HMOR(7) shows a relatively less intense peak, which is decreased by about 20 % compared to the rest of the samples. The same trend is observed also for the peaks corresponding to the $Cu^{I}\cdots(CO)_2$ where the peaks of the 0.18Cu-HMOR (7) appear smaller compared to the other three samples. The intensity of these different peaks corresponds to the amount of CO that can interact with such Cu^{I} species, ultimately providing information on the amount of these species as well as their location, since accessible ions are more prone to interact with CO and form such adducts. Interestingly, the intensities of the peaks in the IR spectra inversely correlate to the activity measurements, as was also seen for the Cu^{I} component peaks observed in the HERFD XANES results. From these observations, it can be suggested that in the case of the highly productive 0.18Cu-HMOR(7), upon high temperature treatment in vacuum or in He, there is a higher amount of a residual Cu^{II}-containing species compared to the other samples. We note how the use of different sample pretreatment protocols (see Sections 2.3 and 2.4), dictated by the specific experimental setups and requirements for FTIR and HERFD XANES spectroscopies, hamper a quantitative correlation between the results obtained with the two techniques. Nonetheless, the two methods are in good qualitative agreement: FITR findings supports that a low temperature reduction-resistant fw-Cu^{II} species is more abundant in this sample, in line with previously reported findings based on HERFD XANES and MCR analysis [15].

3.4. XPS Characterization of 0.18Cu-HMOR(7) and 0.36Cu-HMOR(11)

XPS measurements were also conducted on two Cu-MOR samples with different Si/Al and Cu/Al ratios. In Fig. 4, the XPS Cu 2p spectra of the as-prepared and O_2-activated (10 % O_2/Ar at 500 °C for 3 h) 0.18Cu-HMOR(7) and 0.36Cu-HMOR(11) samples are presented. The two peaks observed at binding energy (BE) in the 933.4–937 eV and 953.5–956 eV ranges correspond to the Cu $2p_{3/2}$ and Cu $2p_{1/2}$ orbitals, respectively. In addition, the two shake-up satellite peaks appear in the 941–945 eV and 962–963 eV ranges, indicating the existence of Cu^{II}-containing species in the investigated zeolites [43]. A BE of 933.5–934.5 eV is commonly found in cupric oxides, but in the case of Cu-exchanged zeolites, slightly positively shifted peaks in the 935.5–936.5 eV BE range have been reported [44,45]. The spectra of Cu $2p_{3/2}$ can be deconvoluted into two peaks, one located at BE ~ 935.8 eV and one at BE ~ 933.6 eV. These have been attributed to isolated Cu^{II} species coordinated to extra framework oxygen (O_{efw}) atoms and agglomerated CuO nanoparticles (NPs) on the surface of catalysts, respectively [46,47]. The absence of CuO clusters has been confirmed for the herein investigated Cu-HMOR samples, based on scanning electron microscopy (SEM) and backscattering electron (BSE) imaging as well as X-ray diffraction and XAS measurements [15,25,26]. Hence, it is a possible that the amount and size of CuO clusters is small and that they are detectable only by XPS, possibly also due to their preferential location at the surface of zeolite micro-crystals. In addition, it has been reported earlier that Cu ions in zeolites with different coordination are found at different BEs; at BE of ~ 934 eV and ~ 936 eV in a tetrahedral and octahedral coordination respectively [48]. $[CuOH]^{+}$ species in zeolites have been recently proposed from DFT to have a high BE around 935.6 eV for this transition [49]. Upon O_2 activation, we observe the intensity of the signals decreasing, consistent with the migration of Cu ions inside the zeolite pore upon calcination. In addition, activation results in a pronounced change in the ratio between the two observed peaks, possibly indicating the transformation of hydrated Cu clusters or $[CuOH]^{+}$ species to isolated Cu^{II}-containing O_2-activated species. The percentage of the peak area of the isolated Cu^{II} species to the total peak area increases from 33 % to 42 % for the 0.18Cu-HMOR(7) and from 27% to 33% for the 0.36Cu-HMOR(11) zeolites after activation.

XPS O 1s spectra collected for the as-prepared and O_2-activated 0.18Cu-HMOR(7) and 036Cu-HMOR(11) samples, are shown in Fig. 5. The peak observed in all the spectra can be deconvoluted in two peaks centered at 531.6 and 533.5 eV. In the as-prepared samples, the main

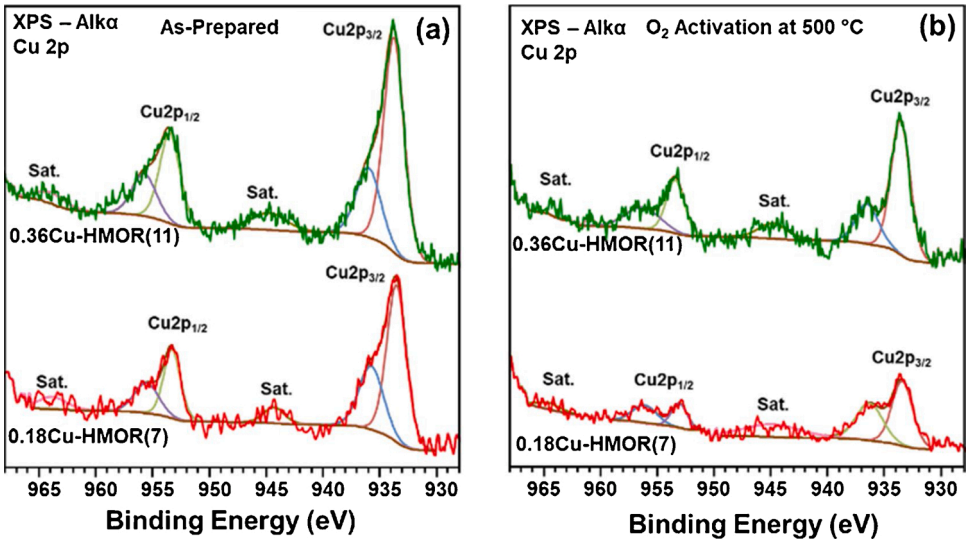

Fig. 4. XPS Cu2p spectra of a) as-prepared (before calcination) and b) after O_2 activation at 500 °C for 180 min for 0.18Cu-HMOR(7) and 0.36Cu-HMOR (11) samples.

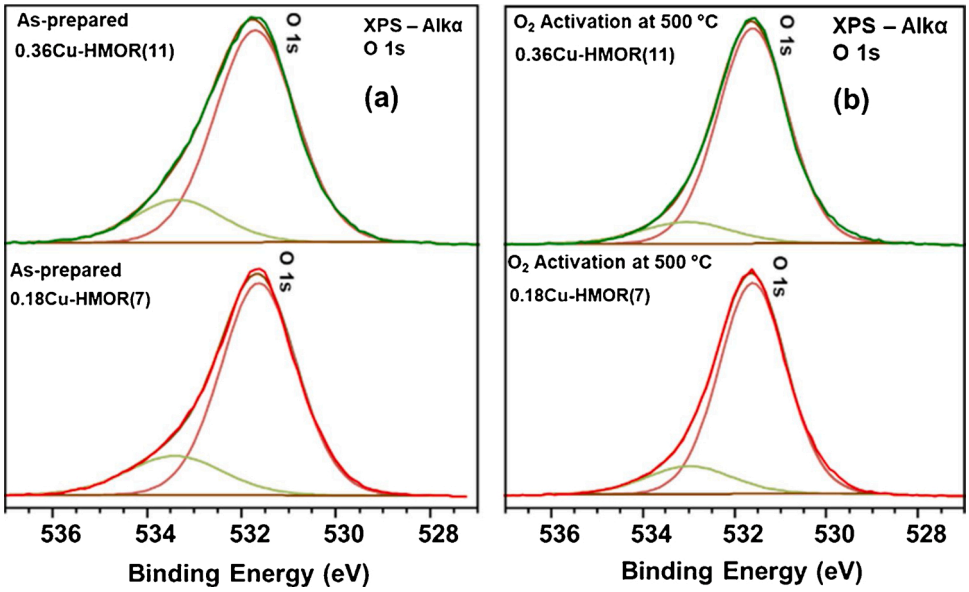

Fig. 5. XPS O 1s spectra of a) as-prepared (before calcination) and b) after O_2 activation at 500 °C for 180 min for 0.18Cu-HMOR(7) and 0.37Cu-HMOR(11) samples.

peak at ~ 531.6 eV is attributed to lattice oxygen species, while the peak at ~ 533.5 eV can be assigned to oxygens belonging to water molecules abundantly present in the as prepared, hydrated, form of the zeolites. After the activation, the spectra appear to be narrower. The second peak shifted to higher BE at ~ 532.9 eV can be assigned to oxygen species bound to Cu ions as a result of O_2 activation [50]. After activation, the percentage of these oxygen species relative to the total O 1s peak is higher in 0.18Cu-HMOR(7) (14.3 %) than in 0.36Cu-HMOR(11) (11.3 %).

3.5. NO_x conversion during NH_3-SCR over Cu-HMOR zeolites

Cu-exchanged zeolites are primarily used as catalysts for the NH_3-SCR of NO_x. Herein, we use NO_x conversion during NH_3-SCR over Cu-HMOR samples as a tool to deepen our understanding of the samples. Three of the four samples were selected, namely 0.18Cu-HMOR(7), 0.28Cu-HMOR(11) and 0.36Cu-HMOR(11), and tested for their NO conversion from 150 to 550 °C using a gas mixture with a composition of 924 ppm NH_3, 903 ppm NO, 8.6 % O_2 in balance of N_2 and He at a GHSV of ~ 19,000 h^{-1}. These process conditions enable observation of clear differences in the low temperature region 150–350 °C. From the results (Fig. 6) it can be seen that there is no activity at 150 °C, but when increasing the temperature, we observe that the sample with the highest Cu loading i.e. 0.36Cu-HMOR(11) shows just above 85 % conversion at 250 °C while the rest of the samples (0.28Cu-HMOR(11) and 0.18Cu-HMOR(7)) are less active at that temperature. Further increase of the temperature results in a conversion increase, with all the samples exhibiting around 100 % NO conversion at 350 °C. Beyond that temperature, the conversion decreases again, indicating the effect of unselective NH_3 oxidation at higher temperatures. The samples with the lower Cu loadings (i.e. 0.18Cu-HMOR(7) and 0.28Cu-HMOR(11)) show a slower decay while the 0.36Cu-HMOR(11) sample shows ~ 80 % conversion at 550 °C. These results indicate that high Cu loadings results in a more active catalyst for the NH_3-SCR reaction. Furthermore, our results are in line with a study by Oord et al. [51] where the authors compared the NO conversion at 200 °C to the DMTM activity of Cu-SSZ-13. It was shown that by increasing the Cu loading, the SCR activity and the DMTM yield both increase. This effects was claimed to be due to higher population of active sites with a higher probability to form dimeric moieties [51]. However, similar observations are not made for Cu-HMOR here, as we only observe an increase in the SCR activity with loading and not in the DMTM activity (see Fig. 1). In our data, the sample with the lowest Cu loading produces more CH_3OH. These findings are likely a result of a specific combination of Cu/Al and Si/Al ratios, as well as synthesis-driven Al distribution in the zeolite framework, promoting the population of the specific fw-Cu^{II} dimeric sites active for the DMTM. Conversely, for NH_3-SCR, the dynamic nature of active sites when exposed to the reaction mixture, involving NH_3-assisted mobilization of Cu-ions, leads to a direct correlation between activity and Cu loading for MOR.

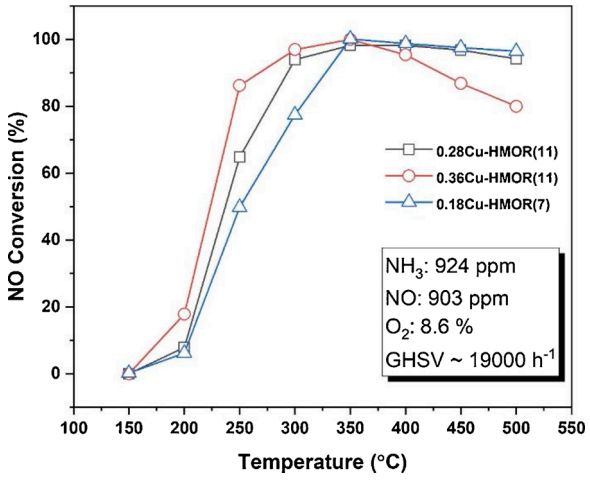

Fig. 6. NO conversion (%) of 0.28Cu-HMOR(11), 0.36Cu-HMOR(11) and 0.18Cu-MOR(7) in the temperature range from 150 to 550 °C. Conditions: 924 ppm NH_3, 903 ppm NO, 8.6 % O_2 and GHSV ~ 19,000 h^{-1}.

Ideally, a complete assessment of SCR performance for the investigated Cu-HMOR material should consider the influence of several other factors, such as surface acid properties and redox ability of catalysts. However, this is beyond the scope of the present work. Nonetheless, the basic observation that the performance ranking of different Cu-MOR materials is different in the two processes clearly demonstrates how the composition/synthesis-dependent Cu speciation in MOR is a key parameter influencing the DMTM activity, but not the NH_3-SCR activity. Indeed, the NH_3-SCR activity appears to depend mostly on the quantity of Cu loaded on the MOR samples, underpinning the fact that interaction with ammonia at low temperature efficiently solvates Cu-ions, driving the catalyst into a quasi-homogeneous state [52] and apparently

resetting the Cu-speciation realized after activation.

4. Conclusions

In this work, we have significantly extended the characterization of a series of Cu-loaded mordenite zeolites that are active for the stepwise, direct conversion of methane to methanol. The key objective has been to further shed light on why one particular sample with Si/Al = 7 and Cu/Al = 0.18 is able to host a much greater fraction of active Cu species than any other material – essentially all Cu species are active for this sample. A central element in our characterization strategy has been to compare materials when activated at 500 °C in either inert He or oxidative O_2 atmosphere. FT-IR spectroscopy with CO as probe molecule and HERFD XANES measurements both demonstrate a high abundance of self-reduction-resistant Cu^{II} species when pretreating the highly active sample in inert atmosphere, which corroborates previous findings based on HERFD XANES and MCR analysis. XPS shows that Cu species migrate from the external zeolite surface and into the micropore system upon activation in oxygen. It appears that hydrated Cu clusters or $[CuOH]^+$ species are converted to isolated Cu^{II} species upon O_2-activation. Moreover, these isolated Cu^{II} species are more abundant for the highly active sample, and this material also has a higher abundance of what might presumably be the activated oxygen species. Finally, the distinct performance of this particular sample is not evident when measuring the NO conversion during NH_3-SCR. Instead, the NH_3-SCR activity follows the Cu loading in a straightforward manner. This demonstrates that, despite the fact that the same zeolite materials are active both for NH_3-SCR and direct methane to methanol conversion, the active site requirements are different.

Declaration of Competing Interest

The authors declare that they have no known competing financial interests or personal relationships that could have appeared to influence the work reported in this paper.

Acknowledgements

The authors acknowledge the iCSI (industrial Catalysis Science and Innovation) Centre for Research-based Innovation, which receives financial support from the Research Council of Norway under contract no. 237922. We also acknowledge R. Baran and P. Glatzel for the support during the HERFD XANES measurements on the ID26 beamline of the ESRF.

References

[1] M.H. Groothaert, P.J. Smeets, B.F. Sels, P.A. Jacobs, R.A. Schoonheydt, J. Am. Chem. Soc. 127 (2005) 1394–1395.
[2] E.M. Alayon, M. Nachtegaal, M. Ranocchiari, J.A. van Bokhoven, Chem. Commun. 48 (2012) 404–406.
[3] M. Ravi, M. Ranocchiari, J.A. van Bokhoven, Angew. Chem. Int. Ed. 56 (2017) 16464–16483.
[4] M.H. Mahyuddin, Y. Shiota, A. Staykov, K. Yoshizawa, Acc. Chem. Res. 51 (2018) 2382–2390.
[5] M. Dyballa, K. Thorshaug, D.K. Pappas, E. Borfecchia, K. Kvande, S. Bordiga, G. Berlier, A. Lazzarini, U. Olsbye, P. Beato, S. Svelle, B. Arstad, ChemCatChem 11 (2019) 5022–5026.
[6] M.H. Mahyuddin, Y. Shiota, K. Yoshizawa, Catal. Sci. Technol. 9 (2019) 1744–1768.
[7] X. Wang, N.M. Martin, J. Nilsson, S. Carlson, J. Gustafson, M. Skoglundh, P. A. Carlsson, Catalysts 8 (2018) 545.
[8] M. Ravi, V.L. Sushkevich, A.J. Knorpp, M.A. Newton, D. Palagin, A.B. Pinar, M. Ranocchiari, J.A. van Bokhoven, Nature Catal. 2 (2019) 485–494.
[9] E.M.C. Alayon, M. Nachtegaal, A. Bodi, J.A. van Bokhoven, ACS Catal. 4 (2014) 16–22.
[10] V.L. Sushkevich, D. Palagin, M. Ranocchiari, J.A. van Bokhoven, Science 356 (2017) 523–527.
[11] V.L. Sushkevich, D. Palagin, J.A. van Bokhoven, Angew. Chem. Int. Ed. 57 (2018) 8906–8910.
[12] S. Grundner, M.A. Markovits, G. Li, M. Tromp, E.A. Pidko, E.J. Hensen, A. Jentys, M. Sanchez-Sanchez, J.A. Lercher Nat. Commun. 6 (2015) 7546.
[13] S. Grundner, W. Luo, M. Sanchez-Sanchez, J.A. Lercher, Chem. Commun. 52 (2016) 2553–2556.
[14] A.J. Knorpp, M.A. Newton, A.B. Pinar, J.A. van Bokhoven, Ind. Eng. Chem. Res. 57 (2018) 12036–12039.
[15] D.K. Pappas, A. Martini, M. Dyballa, K. Kvande, S. Teketel, K.A. Lomachenko, R. Baran, P. Glatzel, B. Arstad, G. Berlier, C. Lamberti, S. Bordiga, U. Olsbye, S. Svelle, P. Beato, E. Borfecchia, J. Am. Chem. Soc. 140 (2018) 15270–15278.
[16] G. Brezicki, J.D. Kammert, T.B. Gunnoe, C. Paolucci, R.J. Davis, ACS Catal. 9 (2019) 5308–5319.
[17] Y. Kuroda, A. Kotani, H. Maeda, H. Moriwaki, T. Morimato, M. Nagao, J. Chem. Soc., Farad. Trans. 88 (1992) 1583–1590.
[18] P. Vanelderen, J. Vancauwenbergh, M.-L. Tsai, R.G. Hadt, E.I. Solomon, R. A. Schoonheydt, B.F, Sels Chemphyschem 15 (2014) 91–99.
[19] P. Vanelderen, B.E. Snyder, M.L. Tsai, R.G. Hadt, J. Vancauwenbergh, O. Coussens, R.A. Schoonheydt, B.F. Sels, E.I. Solomon, J. Am. Chem. Soc. 137 (2015) 6383–6392.
[20] B.E.R. Snyder, P. Vanelderen, R.A. Schoonheydt, B.F. Sels, E.I. Solomon, J. Am. Chem. Soc. 140 (2018) 9236–9243.
[21] E.M.C. Alayon, M. Nachtegaal, A. Bodi, M. Ranocchiari, J.A. van Bokhoven, Phys. Chem. Chem. Phys. 17 (2015) 7681–7693.
[22] J.S. Woertink, P.J. Smeets, M.H. Groothaert, M.A. Vance, B.F. Sels, R. A. Schoonheydt, E.I. Solomon, Proc. Natl. Acad. Sci. U.S.A. 106 (2009) 18908–18913.
[23] E.I. Solomon, D.E. Heppner, E.M. Johnston, J.W. Ginsbach, J. Cirera, M. Qayyum, M.T. Kieber-Emmons, C.H. Kjaergaard, R.G. Hadt, L. Tian, Chem. Rev. 114 (2014) 3659–3853.
[24] D. Palagin, A.J. Knorpp, A.B. Pinar, M. Ranocchiari, J.A. van Bokhoven, Nanoscale 9 (2017) 1144–1153.
[25] M. Dyballa, D.K. Pappas, K. Kvande, E. Borfecchia, B. Arstad, P. Beato, U. Olsbye, S. Svelle ACS Catal. 9 (2019) 365–375.
[26] E. Borfecchia, D.K. Pappas, M. Dyballa, K.A. Lomachenko, C. Negri, M. Signorile, G. Berlier, Catal. Today 333 (2019) 17–27.
[27] D. Bellet, B. Gorges, A. Dallery, P. Bernard, E. Pereiro, J. Baruchel, J. Appl. Crystallogr. 36 (2003) 366–367.
[28] E. Borfecchia, K.A. Lomachenko, F. Giordanino, H. Falsig, P. Beato, A.V. Soldatov, S. Bordiga, C. Lamberti, Chem. Sci. 6 (2015) 548–563.
[29] D.K. Pappas, E. Borfecchia, M. Dyballa, K.A. Lomachenko, A. Martini, G. Berlier, B. Arstad, C. Lamberti, S. Bordiga, U. Olsbye, S. Svelle, P. Beato, ChemCatChem 11 (2019) 621–627.
[30] D.K. Pappas, E. Borfecchia, M. Dyballa, I.A. Pankin, K.A. Lomachenko, A. Martini, M. Signorile, S. Teketel, B. Arstad, G. Berlier, C. Lamberti, S. Bordiga, U. Olsbye, K. P. Lillerud, S. Svelle, P. Beato, J. Am. Chem. Soc. 139 (2017) 14961–14975.
[31] A. Martini, E. Borfecchia, K.A. Lomachenko, I.A. Pankin, C. Negri, G. Berlier, P. Beato, H. Falsig, S. Bordiga, C. Lamberti, Chem. Sci. 8 (2017) 6836–6851.
[32] B. Ravel, M. Newville, J. Synchrotron Radiat. 12 (2005) 537–541.
[33] F.X. Llabrés i Xamena, P. Fisicaro, G. Berlier, A. Zecchina, G.T. Palomino, C. Prestipino, S. Bordiga, E. Giamello, C. Lamberti, J. Phys. Chem. B 107 (2003) 7036–7044.
[34] S.C. Larsen, A. Aylor, A.T. Bell, J.A. Reimer, J. Phys. Chem. 98 (1994) 11533–11540.
[35] V.L. Sushkevich, J.A. van Bokhoven, Chem. Commun. 54 (2018) 7447–7450.
[36] C. Paolucci, A.A. Parekh, I. Khurana, J.R. Di Iorio, H. Li, J.D. Albarracin Caballero, A.J. Shih, T. Anggara, W.N. Delgass, J.T. Miller, F.H. Ribeiro, R. Gounder, W. F. Schneider, J. Am. Chem. Soc. 138 (2016) 6028–6048.
[37] C. Buono, A. Martini, I.A. Pankin, D.K. Pappas, C. Negri, K. Kvande, K. A. Lomachenko, E. Borfecchia Radiat, Phys. Chem. (2018), https://doi.org/10.1016/j.radphyschem.2018.1012.1031.
[38] E.A. Pidko, E.J.M. Hensen, R.A. van Santen, Proc. R. Soc. A-Math. Phys. Eng. Sci. 468 (2012) 2070–2086.
[39] S. Bordiga, C. Lamberti, F. Bonino, A. Travert, F. Thibault-Starzyk Chem, Soc. Rev. 44 (2015) 7262–7341.
[40] M. Iwamoto, Y. Hoshino Inorg, Chem. 35 (1996) 6918–6921.
[41] C. Lamberti, S. Bordiga, M. Salvalaggio, G. Spoto, A. Zecchina, F. Geobaldo, G. Vlaic, M. Bellatreccia, J. Phys. Chem. B 101 (1997) 344–360.
[42] F. Giordanino, P.N.R. Vennestrom, L.F. Lundegaard, F.N. Stappen, S. Mossin, P. Beato, S. Bordiga, C. Lamberti, Dalton Trans. 42 (2013) 12741–12761.
[43] S.P. Wang, X.Y. Wang, J. Huang, S.M. Zhang, S.R. Wang, S.H. Wu, Catal. Commun. 8 (2007) 231–236.
[44] D.C. Frost, A. Ishitani, C.A. McDowell, Mol. Phys. 24 (1972) 861–877.
[45] E.S. Shpiro, W. Grünert, R.W. Joyner, G.N. Baeva, Catal. Lett. 24 (1994) 159–169.
[46] H. Xue, X. Guo, S. Wang, C. Sun, J. Yu, D. Mao, Catal. Commun. 112 (2018) 53–57.
[47] S. Lai, D. Meng, W. Zhan, Y. Guo, Y. Guo, Z. Zhang, G. Lu, RSC Adv. 5 (2015) 90235–90244.
[48] S. Contarini, L. Kevan, J. Phys. Chem. 90 (1986) 1630–1632.
[49] L. Artiglia, V.L. Sushkevich, D. Palagin, A.J. Knorpp, K. Roy, J.A. van Bokhoven, ACS Catal. (2019) 6728–6737.
[50] G. Fu, D. Mao, S. Sun, J. Yu, Z. Yang, J. Ind. Eng. Chem. 31 (2015) 283–290.
[51] R. Oord, J.E. Schmidt, B.M. Weckhuysen, Catal. Sci. Technol. 8 (2018) 1028–1038.
[52] C. Paolucci, I. Khurana, A.A. Parekh, S. Li, A.J. Shih, H. Li, J.R. Di Iorio, J. D. Albarracin-Caballero, A. Yezerets, J.T. Miller, W.N. Delgass, F.H. Ribeiro, W. F. Schneider, R. Gounder, Science 357 (2017) 898.